A model for cyst lumen expansion and size regulation via fluid secretion

Elan Gin, Elly M. Tanaka, Lutz Brusch

www.elsevier.com/locate/yjtbi

A model for cyst lumen expansion and size regulation via fluid secretion

Elan Gin, Elly M. Tanaka, Lutz Brusch

PII: S0022-5193(10)00144-X
DOI: doi:10.1016/j.jtbi.2010.03.021
Reference: YJTBI 5922

To appear in: *Journal of Theoretical Biology*

Received date: 22 January 2010
Revised date: 11 March 2010
Accepted date: 11 March 2010

Cite this article as: Elan Gin, Elly M. Tanaka and Lutz Brusch, A model for cyst lumen expansion and size regulation via fluid secretion, *Journal of Theoretical Biology*, doi:10.1016/j.jtbi.2010.03.021

A model for cyst lumen expansion and size regulation via fluid secretion

Elan Gin [a,*], Elly M. Tanaka [b], Lutz Brusch [a]

[a] *Center for Information Services and High Performance Computing, Dresden University of Technology, 01062 Dresden, Germany*

[b] *DFG Center for Regenerative Therapies, Dresden University of Technology, 01307 Dresden, Germany*

Abstract

Many internal epithelial organs derive from cysts, which are tissues comprised of bent epithelial cell layers enclosing a lumen. Ion accumulation in the lumen drives water influx and consequently water accumulation and cyst expansion. Lumen-size recognition is important for the regulation of organ size. When lumen size and cyst size are not controlled, diseases can result; for instance, renal failure of the kidney. We develop a mechanistic mathematical model of lumen expansion in order to investigate the mechanisms for saturation of cyst growth. We include fluid accumulation in the lumen, osmotic and elastic pressure, ion transport and stretch-induced cell division. We find that the lumen volume increases in two phases: first, due to fluid accumulation stretching the cells, then in the second phase, the volume increase follows the increase in cell number until proliferation ceases as stretch forces relax. The model is quantitatively fitted to published data of *in vitro* cyst growth and predicts steady state lumen size as a function of the model parameters.

Key words: MDCK cyst, chloride secretion, stretch-activated cell proliferation, morphogenesis, mathematical model

* Corresponding author. Tel.: +49 351 463 38780
Email address: elan.gin@tu-dresden.de

1 Introduction

1.1 Importance of cyst size regulation

Organs of the respiratory, digestive, genito-urinary and vascular systems depend on cysts as their building blocks. Cysts are comprised of a bent epithelial cell layer that encloses the lumen and seals it from the extra-cyst medium (O'Brien et al., 2002). Cysts form via mirror-symmetric polarization of adjacent cells, transmembrane protein and channel sorting, directed ion transport and subsequent lumen expansion (Ferrari et al., 2008). Many adult organs derive from cysts during embryonic development and require cyst growth but are also vulnerable to aberrant cell re-arrangements due to deregulated cyst forming mechanisms. For instance, cyst diseases of the kidney are common, in particular autosomal dominant polycystic kidney disease (ADPKD). In ADPKD, multiple fluid-filled cysts develop, grow in size and gradually compress and displace normal nephrons. In early stages of ADPKD, cysts begin to enlarge from many segments of the kidney. The enlarged regions then disassociate from the original nephron to form disconnected cysts. The cysts continue to enlarge due to proliferation of cells and fluid secretion induced lumen expansion. Progressive renal cyst formation and enlargement can result in a loss of renal function and hypertension, which can lead to renal failure (Hanaoka and Guggino, 2000; Sullivan et al., 1998b). The molecular and biophysical feedback loops that control cyst size are of vital interest but remain unknown (Tanner et al., 1992).

The individual mechanisms responsible for cyst growth and size regulation have been studied *in vitro* (Balcarova-Ständer et al., 1984; Tanner et al., 1995) and our mathematical model focuses on corresponding *in vitro* data. The Madin-Darby canine kidney (MDCK) cell line is used extensively to study polar cell functions and ion and fluid transport. This cell line is derived from the renal distal tubular epithelium and has been used to study renal cyst enlargement (Mangoo-Karim et al., 1989). MDCK cells, when seeded in a hydrated collagen gel, divide and form spherical cysts in a period of weeks. The MDCK cysts are lined by a simple, polarized epithelium, with the apical side facing the lumen. The polarity of these cysts is identical to ADPKD cysts or renal tubules, making it a useful model for studying renal cyst enlargement (Tanner et al., 1992). Wang et al. (1990) observe that 5-6 MDCK cells are required to form a lumen, and this occurs around 2 to 3 days after seeding. Zeng et al. (2008) did careful analysis to relate the probability of lumen formation to the number of cells in an aggregate and also found that 5 cells were required for lumen formation. As the cysts grow, the volume of fluid within them increases (McAteer et al., 1987). MDCK cells are also used as a model for epithelial cell growth and morphogenesis. When the MDCK cysts are exposed to mes-

enchymally derived hepatocyte growth factor, they develop branching tubules. This response is similar to epithelial-mesenchymal interactions that stimulate tubulogenesis *in vivo* (O'Brien et al., 2002).

1.2 Mechanisms of cyst growth

In order to initially form a lumen, individual cells must first form the three surfaces: apical, basal and lateral (O'Brien et al., 2002). Once achieved, the polarity of each individual cell must be coupled within the organization of the tissue. The apical surface is orientated towards the lumen. Polarization of MDCK cells in culture is controlled by cell-cell interactions and cell-substratum interactions. The signals that mediate such interactions and the resultant polarization were discussed by Eaton and Simons (1995).

The cysts enlarge due to both proliferation of cells and fluid secretion induced lumen expansion which depends on ion and water channel activity (Ferrari et al., 2008). Recent studies have indicated that cyclic AMP (cAMP) regulates the rate of cell proliferation and fluid accumulation in renal cysts of patients with ADPKD (Belibi et al., 2004; Yamaguchi et al., 2000, 2003). Grown in the absence of cAMP agonists, Mangoo-Karim et al. (1989) found that MDCK cells suspended in collagen failed to form cysts. However, by using cAMP agonists such as forskolin or cholera toxin, Mangoo-Karim et al. (1989) found an increase in cell proliferation as well as higher chloride levels in the cyst fluid.

Fluid accumulation in the lumen is the result of fluid secretion driven by active transepithelial Cl^- secretion into the lumen. Cl^- secretion is mediated via cystic fibrosis transmembrane conductance regulator (CFTR) Cl^- channels in the apical membrane. Studies by Li et al. (2004) showed that when the Cl^- channel was blocked, a negative effect on cyst growth was observed, through the inhibition of the channels. Fluid accumulation within the lumen was then inhibited.

Tanner et al. (1995) studied the effects of mechanical stretch on cell proliferation. Their findings showed that proliferation increases to accommodate the increased membrane surface area. Once cell number had increased, DNA synthesis returned to baseline. A possible mechanism is suggested by the observation that stretched fetal lung cells release a diffusible growth factor causing unstretched cells to proliferate (Liu et al., 1993). However, Tanner et al. (1995) did not find such a diffusible signal for MDCK cells. Stretch-activated cell proliferation has also been studied theoretically by Shraiman (2005) who developed a mathematical model of mechanical deformation in the growing tissue of a *Drosophila* wing imaginal disc in order to understand the control

of growth rate. The simulations showed that clones growing faster or slower than the surrounding tissue are subject to mechanical stress. This stress may provide a feedback signal to cells, regulating cell division and self-organizing the uniformly distributed growth of the tissue (Nienhaus et al., 2009).

We also draw on two previously published models of lumen expansion and fluid secretion. Kücken et al. (2008) developed a model for the onset of regeneration of the freshwater polyp *Hydra*. A small fragment of tissue can regenerate into a complete animal in approximately 48 hours. To do this, the tissue forms a hollow sphere made of a cell bilayer. Once the hollow sphere has been formed, it undergoes cycles of inflation and collapse. Kücken et al. (2008) modeled this process where the inflation of the sphere is controlled by an osmotic pressure and an elastic pressure. The osmotic pressure is affected by the difference in the ionic concentrations within the sphere and outside of the sphere. They included a constant influx of ions into the sphere. The expansion is arrested by including tissue rupture and a collapse of the sphere.

Physiological models have been proposed by Tanner et al. (1992); Sullivan et al. (1998a); Li et al. (2004) which describe ion transport mechanisms. These types of mechanisms were included by Gin et al. (2007) who modeled fluid secretion in parotid acinar cells. In more detail, fluid accumulation within the lumen is regulated by the ionic concentration differences between the lumen, the cell interior and the extracellular medium. The intracellular ionic concentration is controlled by different ion transport mechanisms, such as K^+ and Cl^- channels, $Na^+-K^+-2Cl^-$ cotransporters and Na^+-K^+-ATPase ion exchangers. The increased ionic concentration in the lumen lead to water flux from the cell into the lumen. In their model the Cl^- channel was dependent on the intracellular $[Ca^{2+}]$. Intracellular Ca^{2+} signaling pathways were also modeled such that stimulation by an agonist which lead to increased intracellular $[Ca^{2+}]$ translated to an increased water flow into the lumen due to higher lumenal Cl^- accumulation.

In this study, we investigate the feedback mechanisms by which the growth of the cyst can saturate and shed light on organ size regulation in this simple tissue. A system of ordinary differential equations is developed and analyzed to describe the expansion of the lumen via both cell proliferation and fluid accumulation. In the next section, we derive this model and fit its parameters to published experimental data. We do not model the initial formation of a lumen and will initialize our model at the earliest stage when a cyst has just developed and a lumen has already been formed. In section 3 we analyze the cyst growth dynamics and explore the role of individual feedback loops. We conclude with insight on the asymptotic cyst size and a discussion of future steps.

2 The model

In this section, we describe the features of the mathematical model for cyst lumen expansion. The three variables of the model are the lumen volume, $w_l(t)$, the lumenal Cl^- concentration, $[Cl^-](t)$, and the number of cells, $c(t)$.

Fig. 1 shows the feedback mechanisms that we will include in our model. Cl^-

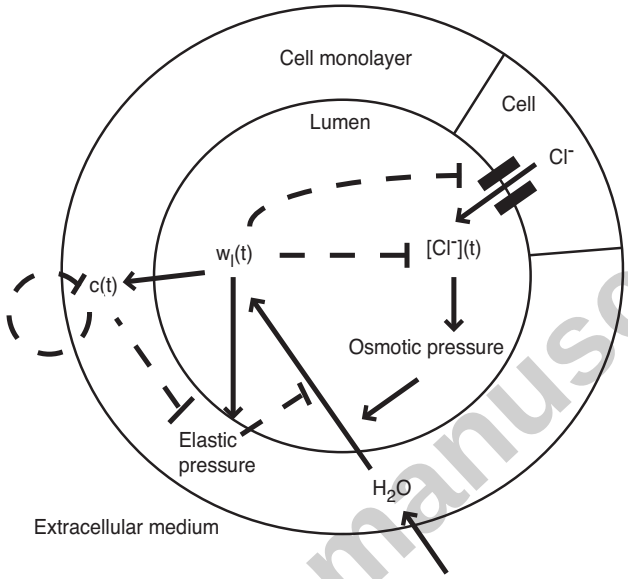

Fig. 1. Mechanisms of lumen volume expansion. Dashed lines indicate negative feedback mechanisms. Solid lines with arrowheads indicate positive feedback mechanisms. One individual cell is shown.

enters the lumen via Cl^- channels located on the apical membrane of the cells. The increased $[Cl^-]$ increases the osmotic pressure, causing water influx into the lumen. The water accumulation in the lumen leads to lumen volume expansion. On a slower time scale, the increased lumen volume promotes cell division. Cell number is decreased via cell death or cells migrating out of the monolayer. The increased cell number decreases the elastic pressure. Long-term, the increasing lumen volume will dilute the $[Cl^-]$ in the lumen, leading to saturation of the $[Cl^-]$ with the effect of saturating the lumen volume.

The changes in the lumen volume ($w_l(t)$), lumenal $Cl^-(t)$ concentration and the number of cells ($c(t)$) can all be described by ordinary differential equations. We derive each of these in the following subsections. Our strategy is to first include into the model many regulatory interactions as described in the experimental literature and then later to explore the dynamics of reduced models by setting individual terms and parameters to zero.

2.1 Lumen volume expansion

Fluid accumulation within the lumen is one mechanism by which lumen expansion occurs. The water flow is driven by the osmotic pressure resulting from the ion concentration difference between the lumen and cellular compartments and the opposing elastic pressure of the cyst monolayer.

The rate of change in the lumen volume is described by the following equation:

$$\frac{dw_l}{dt} = L_{\mathrm{w}} A_{\mathrm{apical}} c(t) \Delta P, \tag{1}$$

where L_{w} is the water permeability coefficient, A_{apical} is the surface area of the apical membrane of a single cell (which is assumed to remain constant), and $c(t)$ is a variable describing the number of cells (equation given in the next section).

The driving force for fluid influx is found from the difference ΔP of the osmotic pressure and the elastic pressure:

$$\Delta P = RT(C_{\mathrm{lumen}} - C_{\mathrm{intra}}) - \frac{4(R_l(t) - R_r(t))\tilde{E}}{R_r(t)^2}, \tag{2}$$

for $R_l(t) > R_r(t)$ (the lumen radii $R_l(t)$ and $R_r(t)$ are described later). The parameter R is the molar gas constant and has the value 8.315 J mol^{-1} K^{-1} (or Pa K^{-1}(mol/m^3)$^{-1}$) and T is set to body temperature, 310 K.

The first term of ΔP describes the osmotic pressure with C_{lumen} being the concentration of ions in the lumen and C_{intra} the ionic concentration in the cell. The terms C_{intra} (intracellular ion concentration) and C_{lumen} (lumenal ion concentration) are given by:

$$C_{\mathrm{intra}} = ([\mathrm{Cl}^-]_i + [\mathrm{Na}^+]_i + [\mathrm{K}^+]_i + [\mathrm{X}]), \tag{3}$$
$$C_{\mathrm{lumen}} = ([\mathrm{Cl}^-]_l(t) + [\mathrm{Na}^+]_l + [\mathrm{K}^+]_l), \tag{4}$$

where [X] is the concentration of impermeable ions and the subscripts i and l denote intracellular and lumen, respectively. The lumenal sodium concentration, $[\mathrm{Na}^+]_l$, and potassium concentration, $[\mathrm{K}^+]_l$, are assumed to be equal to the extracellular sodium concentration, $[\mathrm{Na}^+]_e$, and potassium concentration, $[\mathrm{K}^+]_e$, respectively. We also keep the intracellular ion concentrations fixed, assuming that their dynamics is on a timescale of seconds (Gin et al., 2007), whereas the lumen increase follows a timescale of hours. We assume that there is a concentration gradient between the cellular and extracellular compartments, such that there is always water flow into the cell (Gin et al., 2007).

Eq. 1 describes water flow via a transcellular pathway as found by Rivers et al. (1996) who studied populations of MDCK cysts. This was also found to be the case by Kovbasnjuk et al. (1998) who developed an optical microscopic technique to visualize the flow velocity profiles within the lateral intercellular spaces and to test for fluid flow across the tight junction. The flow velocity within the lateral intercellular spaces fell almost to zero adjacent to the tight junction, indicating that transjunctional flow can be neglected.

The second term of ΔP describes the elastic pressure. The elastic pressure term is given by

$$\frac{4(R_l(t) - R_r(t))\tilde{E}}{R_r(t)^2} \tag{5}$$

where the elasticity of the cell monolayer is approximated as linear dependence in agreement with the model of Kücken et al. (2008). Here $\tilde{E} = Eh/(2(1-\mu)$, where E is Young's modulus, h is the thickness of the cell monolayer and μ is Poisson's ratio.

The lumen radius is given by $R_l(t)$, and is calculated directly from the lumen volume by approximating the lumen as a sphere. The relaxed lumen radius $R_r(t)$ describes an unstretched cyst with the same number of cells. Details for calculating the radii are described later.

2.2 Cell number changes

Tanner et al. (1995) found that the stretched cells of expanding cysts increased their proliferation rate and proliferated until the characteristic cell number per unit lumen surface was restored. This was described as a stretch-induced proliferation mechanism for cyst enlargement. Stretch-induced proliferation has since been characterized *in vivo* and *in vitro* (Tan et al., 2003; Shraiman, 2005; Nienhaus et al., 2009). Taking these observations into account, the rate of change in cell number can be described as follows:

$$\frac{dc}{dt} = \frac{c(t)\Delta A\gamma_{\mathrm{db}}}{A_{\mathrm{apical}}} - c(t)\gamma_{\mathrm{d}}, \tag{6}$$

where γ_{db} is the doubling rate of cells. The term $-c(t)\gamma_{\mathrm{d}}$ describes the net effect of stretch-independent proliferation and loss of cells due to death or migration out of the monolayer. In the case where the term is negative, as it is here for positive γ_{d}, the death process outweighs stretch-induced cell proliferation. A stretch-activation mechanism, ΔA, which gives the response to an increase in

the difference between the surface area of the lumen, $A(t)$, and the surface area covered by relaxed cells, is given by:

$$\Delta A = A(t) - c(t)A_{\text{apical}}. \tag{7}$$

The surface area of the lumen is calculated from the lumen radius, $R_l(t)$, by assuming a spherical lumen:

$$A(t) = 4\pi R_l(t)^2. \tag{8}$$

2.3 Lumenal chloride concentration changes

The build up of $[Cl^-]$ in the lumen occurs via the influx through apical Cl^- channels. The accumulation of Cl^- in the lumen creates a concentration gradient and water flows from a region of high water concentration to a region of lower water concentration across the apical membrane of the cell.

The term I_{Cl} gives the chloride ion flux from all the cells into the lumen:

$$I_{\text{Cl}} = g_{\text{Cl}} c(t) P_{\text{Cl}} (V_m - V_{\text{Cl}}) P_{\text{sd}}, \tag{9}$$

where g_{Cl} is the maximum whole cell conductance for Cl^-,

$$V_{\text{Cl}} = \frac{RT}{z_{\text{Cl}} F} \log\left(\frac{[\text{Cl}^-]_l(t)}{[\text{Cl}^-]_i}\right) \tag{10}$$

is the Nernst potential for Cl^-, RT is as in Eq. 2, $T = 310$ K, $F = 96490$ C mol^{-1} and $z_{\text{Cl}} = -1$ is the valence for Cl^-. The open probability of the channel is given by P_{Cl}, which we take to be constant. The open probability normally describes the gating mechanism of the chloride channel and could be ligand or voltage dependent. However, we do not include any such mechanisms. The driving force, $V_m - V_{\text{Cl}}$ is assumed to be linear, where V_m is the constant apical membrane potential of the cell.

Cells maintain their volume by activation of ion conductances such that the loss of ions causes a passive flow of water, decreasing the cell volume (Sardini et al., 2003). In particular, activation of a chloride conductance upon swelling is a key step in regulating cell volume. We test a similar idea by incorporating a stretch-deactivation mechanism for the Cl^- channel. However, as discussed in a later section, the qualitative results do not depend on this stretch dependence. The stretch-deactivation is given by the following term:

$$P_{\mathrm{sd}} = 1 - \frac{\Delta A}{\Delta A + k_p}, \tag{11}$$

where ΔA gives the degree of surface stretching as defined in Eq. 7. When ΔA is large, compared to k_p, giving $P_{\mathrm{sd}} < 1$, the chloride channels are deactivated. This stretch dependence can also be interpreted as the average effect of temporally periodic ion transport that is modulated by stretch-dependent cell cycles.

We also include an efflux of Cl^- from the lumen. Tanner et al. (1992) found that chloride moved out of the cyst lumen via a paracellular pathway, by investigating the effects of the small molecule DIDS, known to inhibit the uptake of cAMP in human red blood cells. They speculated that if chloride did leave via a transcellular route, a decreased rate of fluid absorption in the presence of DIDS would result. However, as fluid absorption was unaffected by DIDS, they concluded that chloride moves out of the cyst lumen mainly via a paracellular pathway. We include a corresponding leak of Cl^- ions from the lumen:

$$J_{\mathrm{leak}} c(t)([\mathrm{Cl}^-]_l - [\mathrm{Cl}^-]_e), \tag{12}$$

which is proportional to the number of junctions between cells and correspondingly to the number of cells, $c(t)$ and the concentration difference between the lumenal $[Cl^-]$ and the extracellular $[Cl^-]$.

Combining the above mechanisms regulating the $[Cl^-]$, we arrive at the following equation for the rate of change of the lumenal Cl^- ion number $[\mathrm{Cl}^-]_l w_l$:

$$\frac{d([\mathrm{Cl}^-]_l w_l)}{dt} = w_{\mathrm{cell}} \frac{I_{\mathrm{Cl}}}{z_{\mathrm{Cl}} F} - w_l(t) J_{\mathrm{leak}} c(t)([\mathrm{Cl}^-]_l - [\mathrm{Cl}^-]_e), \tag{13}$$

where w_{cell} is the constant cell volume. This equation obeys mass conservation while lumen volume is changing.

By expanding the equation for the lumen chloride concentration, we obtain the third term capturing the diluting effect of lumen expansion on Cl^- concentration ($[Cl^-]$ is easier measurable experimentally than the total ion number):

$$\frac{d([\mathrm{Cl}^-]_l)}{dt} = \frac{w_{\mathrm{cell}}}{w_l(t)} \frac{I_{\mathrm{Cl}}}{z_{\mathrm{Cl}} F} - J_{\mathrm{leak}} c(t)([\mathrm{Cl}^-]_l - [\mathrm{Cl}^-]_e) - \frac{[\mathrm{Cl}^-](t)}{w_l(t)} \frac{dw_l(t)}{dt}. \tag{14}$$

2.4 Lumen radius

To determine the elastic pressure, the lumen radii, given by $R_r(t)$ and $R_l(t)$, are required. Here, R_r describes the relaxed, non-stretched radius. Kücken et al. (2008) assume that the relaxed radius R_r is constant (they use the variable R_0 and refer to it as the initial radius) as there is no evidence for cell divisions occurring during early (cyst-like) *Hydra* regeneration. However, this is not the case for MDCK cells and thus, an algebraic equation is included to describe the increase of $R_r(t)$ as a function of the number of cells, $c(t)$, and the constant, relaxed apical surface area per cell that they cover:

$$R_r(t) = \left(\frac{c(t)A_{\text{apical}}}{4\pi}\right)^{1/2}. \tag{15}$$

The radius of the lumen, $R_l(t)$, is calculated directly from the lumen volume by approximating the lumen by a sphere:

$$R_l(t) = \left(\frac{3}{4\pi}w_l(t)\right)^{1/3}. \tag{16}$$

2.5 Complete system of equations

The complete system of equations we solve is summarized here. Three nonlinear ordinary differential equations describe the cyst growth dynamics:

$$\begin{aligned}
\frac{dw_l}{dt} &= L_{\text{w}}A_{\text{apical}}c(t)\Delta P,\\
\frac{dc}{dt} &= \frac{c(t)\Delta A\gamma_{\text{db}}}{A_{\text{apical}}} - c(t)\gamma_{\text{d}},\\
\frac{d([\text{Cl}^-]_l)}{dt} &= \frac{w_{\text{cell}}}{w_l(t)}\frac{I_{\text{Cl}}}{z_{\text{Cl}}F} - J_{\text{leak}}c(t)([\text{Cl}^-]_l - [\text{Cl}^-]_e) - \frac{[\text{Cl}^-](t)}{w_l(t)}\frac{dw_l(t)}{dt},
\end{aligned} \tag{17}$$

which are coupled via the following algebraic equations:

$$
\begin{aligned}
\Delta P &= RT(C_{\text{lumen}} - C_{\text{intra}}) - \frac{4(R_l(t) - R_r(t))\tilde{E}}{R_r(t)^2}, \\
\Delta A &= A(t) - c(t)A_{\text{apical}}, \\
A(t) &= 4\pi R_l(t)^2, \\
R_l(t) &= \left(\frac{3}{4\pi} w_l(t)\right)^{1/3}, \\
R_r(t) &= \left(\frac{c(t)A_{\text{apical}}}{4\pi}\right)^{1/2}, \\
C_{\text{intra}} &= ([\text{Cl}^-]_i + [\text{Na}^+]_i + [\text{K}^+]_i + [\text{X}]), \\
C_{\text{lumen}} &= ([\text{Cl}^-]_l(t) + [\text{Na}^+]_l + [\text{K}^+]_l), \\
I_{\text{Cl}} &= g_{\text{Cl}} c(t) P_{\text{Cl}} (V_m - V_{\text{Cl}}) P_{\text{sd}}, \\
P_{\text{sd}} &= 1 - \frac{\Delta A}{\Delta A + k_p}.
\end{aligned} \tag{18}
$$

2.6 Parameter values

Where available, we fix parameter values to experimentally measured values reported in the literature. The remaining parameters are then fitted to experimental data by Wang et al. (1990).

Water permeability (P_f) values have been measured experimentally. Rivers et al. (1996) measure a value of 2.4 μm s^{-1}, while Timbs and Spring (1996) measure both the basolateral and apical cell membrane water permeabilities and find both membranes exhibit permeabilities of 0.001 cm s^{-1} for MDCK cells. Farinas and Verkman (1996) used a method of interferometry to measure cell shape and volume to measure the P_f in cell layers and obtained a value of 6.1×10^{-4} cm s^{-1}. In order to convert a water permeability of units cm s^{-1} to cm (s atm)$^{-1}$, we use the relation $L_w = P_f V_w/(RT)$ (Fischbarg et al., 1993), where P_f is the water permeability coefficient expressed in units of cm s^{-1}, and V_w is the molar volume of water. We chose a water permeability value of 6×10^{-13} cm (s atm)$^{-1}$, which corresponds approximately to a value for P_f of 8.59×10^{-5} cm s^{-1}.

Individual cell apical surface area is calculated from an estimate of the initial lumen volume and the minimum number of cells required for lumen formation. We calculated a value of 52.62 μm^2 from the measurements of (Wang et al., 1990). A value of 57.2 μm^2 is given by Timbs and Spring (1996) for the average smooth surface area. We assume the cell apical surface area to remain constant and take this measurement to represent the surface area when the cell cytoskeleton is relaxed.

The cell volume, $w_{\text{cell}} = 420.92\mu\text{m}^3$ is calculated from the apical surface area

and an assumed cell length (defined to be the distance between the apical membrane and the basal membrane) of 8 μm. We estimated, approximately, the cell length from the images of Elia and Lippincott-Schwartz (2009). Because the cyst is made up of only a monolayer of cells, the cell length is also the thickness of the monolayer (denoted by the parameter h in Eq. 5).

The value of $\tilde{E}$ was taken from Kücken et al. (2008), 0.1 Nm^{-1}.

For the intracellular and extracellular ion concentrations, we refer to Mangoo-Karim et al. (1989) who measured the ionic composition of both secreted fluid (MDCK monolayers) and cyst fluid (MDCK cysts). The medium concentrations, corresponding here to $[\mathrm{Cl}^-]_e$, $[\mathrm{Na}^+]_e$ and $[\mathrm{K}^+]_e$, are 123 mM, 162 mM and 4.4 mM, respectively. Using electron probe analysis, they measure the cyst fluid concentrations of $[\mathrm{Cl}^-]_l$ = 138 mM, $[\mathrm{Na}^+]_l$ = 159 mM and $[\mathrm{K}^+]_l$ = 4.7 mM. The increase in the $[\mathrm{Cl}^-]_l$ is consistent with active transport of Cl^- into the lumen. We assume the lumenal $[\mathrm{Na}^+]$ and $[\mathrm{K}^+]$ are equal to the extracellular values, given the small difference found by Mangoo-Karim et al. (1989). The value of the intracellular impermeable ions, [X], was chosen to give a long-term steady-state lumen $[\mathrm{Cl}^-]$ of approximately 15 mM higher than the extracellular Cl^- concentration, $[\mathrm{Cl}^-]_e$, (Mangoo-Karim et al., 1989). In our model, the steady-state concentration of Cl^- in the lumen is 132.55 mM.

Stefani and Cereijido (1983) found the cells to have an intracellular potential of -40.5 mV although they reported that the actual value may be higher at -50 mV due to leaks around the microelectrode, mechanical damage to the cell or perturbations due to the handling of the preparation. They also investigated the possibility of cell-cell coupling and found that the cells are not electrophysiologically connected. Therefore, we are able to treat each cell as a single unit and choose a membrane potential, $V_m = -50$ mV.

The remaining parameters, g_{Cl}, k_p, J_{leak} and γ_{db} were fitted to the data of Wang et al. (1990) who measure the cyst diameter. They suspended single MDCK cells in type I collagen gel and found the growth to consist of two stages. The first stage occurs between days 1 and 3 in culture and during this time, the cells undergo two to three cell divisions. In this stage, there is no evidence of a lumen. The second stage occurs after this time and the cell aggregates form a central lumen. In order to compare our results with theirs, we assume that all cell divisions occur in the plane of the epithelium so that the cyst consists of only a single layer of cells. By assuming an initially unstretched situation in the experiment, we obtain the lumen radius by dividing the experimental diameter by two and subtracting the cell length, set at 8 μm. Cysts are generally found to remain spherical (McAteer et al., 1987) and thus, we can easily obtain the cyst volume. We also estimated the standard deviation, σ, from their measurements. Table 1 gives the experimental measurements to which we fit the parameters of the model. Wang et al. (1990) found it was not till day 3 that

Experiment time (days)	Model time (days)	Lumen volume (μm^3)	σ (μm^3)
3	0	4.01×10^2	7.0×10^1
4	1	9.9×10^3	1.3×10^3
5	2	6.0×10^4	8.8×10^3
6	3	1.0×10^5	2.4×10^4
7	4	8.9×10^4	2.1×10^4
8	5	1.2×10^5	1.6×10^4
9	6	3.1×10^5	6.2×10^4
	9	3.1×10^5	1.1×10^4
	14	3.1×10^5	1.1×10^4

Table 1
Experimental lumen calculated from volume measurements by Wang et al. (1990) used to fit the model parameters. The standard deviation is given by σ. Wang et al. (1990) found it was not till day 3 that a lumen developed. Their measurement at day 3 was taken to be our initial lumen volume at the start time of the model dynamics The data is plotted in Fig. 2.

a lumen developed. Our model description starts at the stage at which a lumen has already formed, so we take their measurement at day 3 to be our initial lumen volume. Wang et al. (1990) also find that growth stops after eight or nine days and the cyst remains viable for several weeks. Therefore we include two additional data points, days 9 and 14, with identical lumen volume in order to represent the steady lumen volume. We use a smaller σ value for these two added data points to restrict the parameter fitting so that the simulated lumen volume saturates close to the observed value. The parameters were fitted using a Bayesian inference and Markov chain Monte Carlo (MCMC) method. In the Bayesian approach, the parameters are assumed to be random variables that follow a particular distribution. Inferences are made based on the posterior distribution of the parameters, given the data. Prior information about the parameters is also taken into account. The MCMC method provides a means of generating a sample from the posterior distributions of the parameters given the data. The advantage of this technique is that we can obtain statistical information about the fit, such as the maximum, the mean, or any other statistic of the fitted parameter values. Further details of this fitting technique are given in the Appendix.

A summary of all the parameter values is given in Table 2.

Cell parameters			
L_{w}	6.0×10^{-13} cm (s atm)$^{-1}$	$\tilde{E}$	0.1 N m^{-1}
R	8.315 J (K mol)$^{-1}$	T	310 K
A_{apical}	52.62 μm^2	w_{cell}	420.92 μm^3
Intracellular ion concentrations			
$[\mathrm{Cl}^-]_i$	60.0 mM	$[\mathrm{Na}^+]_i$	15.0 mM
$[\mathrm{K}^+]_i$	150.0 mM	[X]	62.50 mM
Extracellular ion concentrations			
$[\mathrm{Cl}^-]_e$	115.0mM	$[\mathrm{Na}^+]_e$	150.0 mM
$[\mathrm{K}^+]_e$	5.0 mM		
Lumen ion concentrations			
$[\mathrm{Na}^+]_l$	150.0 mM	$[\mathrm{K}^+]_l$	5.0 mM
Membrane potential			
V_m	-50 mV		
Lumenal $[\mathrm{Cl}^-]$ parameters			
g_{Cl}	7.30 nS ($\pm$1.61)	z_{Cl}	-1
k_p	403.38 μm^2 ($\pm$68.15)	J_{leak}	5255.63 hr^{-1} ($\pm$1529.94)
P_{Cl}	0.1	F	96490 C mol^{-1}
Cell proliferation parameters			
γ_{db}	8.677×10^{-4} μm^{-2}hr^{-1} ($\pm 8.28 \times 10^{-5}$)	γ_{d}	0.01 hr^{-1}

Table 2
Parameter values for model equations. The parameters $g_{\mathrm{Cl}}, k_p, J_{\mathrm{leak}}, \gamma_{\mathrm{db}}$ were fitted using a Bayesian inference and Markov chain Monte Carlo (MCMC) method (described in the Appendix). Standard deviations for the fitted parameter values are also given.

3 Model simulation

Our aim is to investigate the regulatory mechanisms which arrest lumen growth and thereby control cyst size. We are interested in particular, in the lumenal Cl^- accumulation which drives water flux, and cell proliferation as the mechanisms for lumen expansion. Correspondingly we study, in the following

subsections, stretch-induced responses, the role of cell death, non-saturating lumen growth scenarios and the dependence of asymptotic cyst size on Cl^- transport.

As an initial condition, we use the experimental data at day 3 of the experiments by Wang et al. (1990) when the lumen has just been formed. This fixes the number of cells at five and gives an initial radius of the lumen, R_l, of 4.58 μm, from which we calculate the initial lumen volume. All initial values for the simulation are: $w_l = 401.23\ \mu m^3$, $c = 5$ and $[Cl^-]_l = 115$ mM.

Fig. 2 shows the experimental values used to fit the parameters and the simulated lumen volume curve. More details are given in the following section.

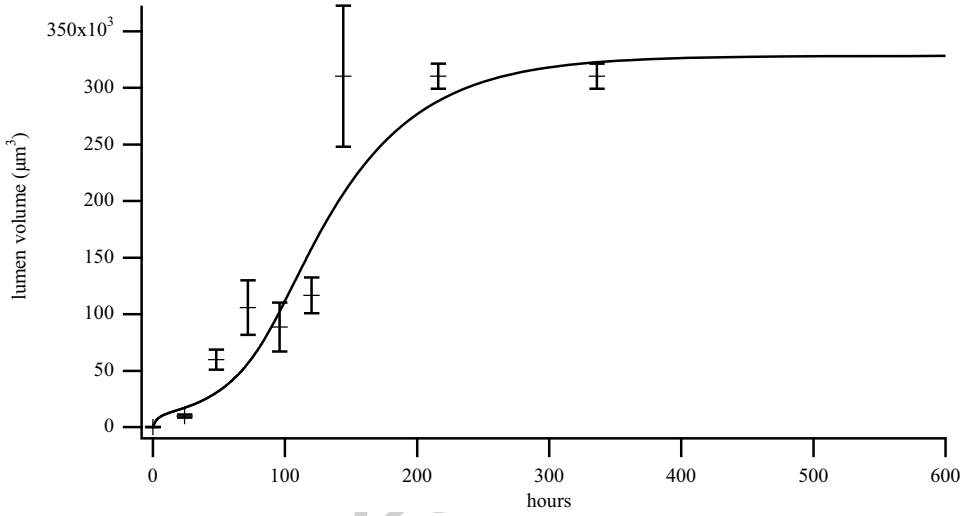

Fig. 2. Simulated lumen volume (solid) curve for parameters fitted to the experimental measurements (symbols) obtained from Wang et al. (1990), given in Table 1. Lumen volume remains stationary from 400 hours onward.

3.1 Stretch-induced responses

We investigate here the effects of stretch on both the deactivation of the Cl^- channels and stimulation of cell proliferation, and their impact on lumen volume expansion.

Fig. 3 shows the model simulation results. Panel A shows the simulated lumen volume (solid curve) along with the experimental values (symbols). We find that the Cl^- influx is extremely rapid, with the $[Cl^-]$ reaching a maximum concentration of 386.77 mM, shown in Fig. 3B. The $[Cl^-]$ then drops rapidly

to approximately 150 mM by 6 minutes The cell number increases on a slower time scale.

This fast increase in the [Cl^-] translates into a rapid increase of the lumen volume (Panel A) and the lumen radius, $R_l(t)$ (Panel D, dashed curve). The two radii, $R_l(t)$ and $R_r(t)$ are shown in Fig. 3D on the left axis. The relaxed radius, $R_r(t)$ (dotted curve) increases much slower, as it is given by the number of cells. This can be seen from the solid curve, giving the quantity $R_l(t) - R_r(t)$. The volume expansion rate is initially proportional to the [Cl^-], as shown in

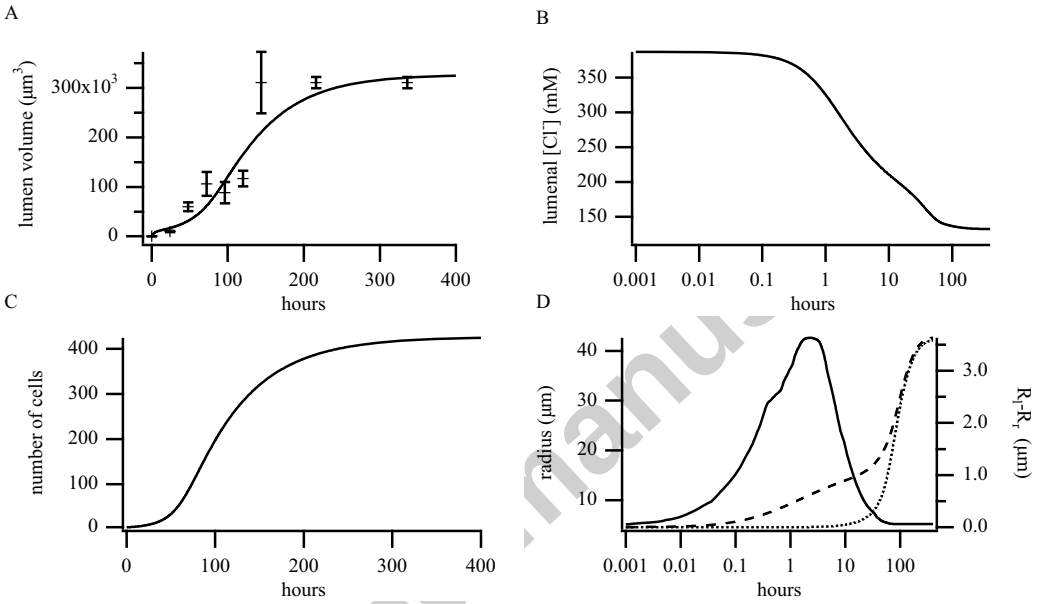

Fig. 3. A: Lumen volume. Model simulation is given by the solid curve. Experimental values fitted are from Wang et al. (1990). The mean volume and standard deviation are shown. B: Lumenal [Cl^-]. C: cell number. D: Radii. Lumen radius, $R_l(t)$ (dashed curve, left axis), relaxed radius, $R_r(t)$ (dotted curve, left axis). The difference $R_l - R_r$ is shown as the solid curve corresponding to the right axis.

Fig. 4A. The lumen volume derivative is shown as the solid curve. As the lumenal [Cl^-] drops, the rate of lumen increase also decreases. While the [Cl^-] continues to drop, the lumen volume has a second growth phase, dependent on the rate of change in the cell number (Fig. 4B, dashed curve). The cell number increase is initially slow, but at approximately 10 hours, increases strongly. This gives a corresponding increase in the rate of lumen increase. One can also see the two growth phases in Fig. 2. The lumen volume saturates at a value of 3.281 $\times 10^5$ μm^3.

Analytically, we can calculate the steady-state lumen volume:

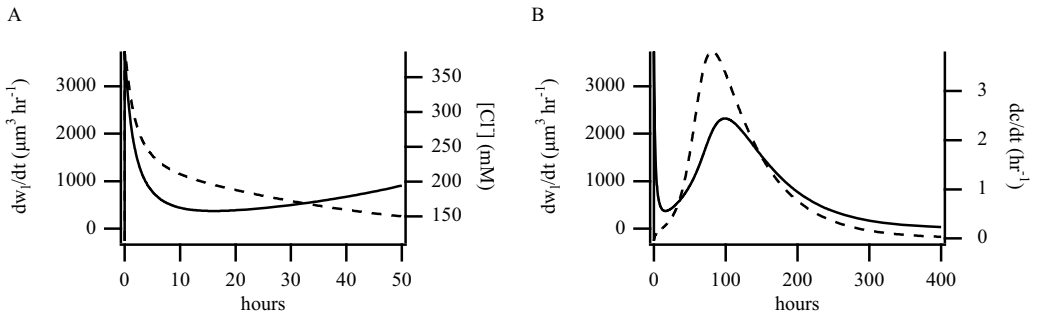

Fig. 4. Lumen volume increases in two stages. Lumen volume derivative is given by the solid curve on both panels (left axis). A: The $[Cl^-]$ is shown by the dashed curve (right axis). This result is shown up to 50 hours. B: The cell number derivative is given by the dashed curve (right axis).

$$w_l = \frac{4\pi}{3\sqrt{(4\pi)^3}} A_{\text{apical}}^{3/2} \left(\frac{\gamma_{\text{d}}}{\gamma_{\text{db}}} + c \right)^{3/2} . \tag{19}$$

From the sum in this equation, it is seen that the steady-state lumen volume has two contributions. The first is given by the stretch of a given number of cells, at steady state equal to $\gamma_{\text{d}}/\gamma_{\text{db}}$, and the second by the final number of cells, c.

Cell doubling times are calculated from our model simulations of $c(t)$ and we find the doubling time between 50 and 100 hours to be 18.49 hours, between 100 and 150 hours, a doubling time of 61.76 hours is obtained and between 150 and 200 hours, the doubling time is 190.77 hours.

The changes in the $[Cl^-]$ are influenced by both the changes in the lumen volume and the stretch-deactivation of the channels. Both these terms are shown in Fig. 5. The stretch-deactivation term, P_{sd} (dashed curve, right axis), transiently drops and at approximately 100 hours, increases. A value of one corresponds to maximum Cl^- flux. However, at this stage, it can be seen that though the Cl^- channels are at their maximum open probability, the $[Cl^-]$ does not increase further. This is due also to the expansion of the lumen diluting the $[Cl^-]$. The ratio of the total cell volume to the lumen volume, $w_{\text{cell}}c(t)/w_l(t)$, denoted by γ_{L} is shown in Fig. 5B (dashed curve, right axis). Initially, the total cell volume is greater than the lumen volume. However, this ratio decreases, rapidly, contributing to the dilution of $[Cl^-]$ in the lumen. At approximately 10 hours, the ratio increases slightly. However, this effect is not enough to increase the $[Cl^-]$, which continues to decrease. This is also affected by the stretch-deactivation of the Cl^- channels so that there is less Cl^- influx from the cells into the lumen.

The saturation of the lumen occurs when the pressure term, ΔP is zero. Interestingly, the osmotic and elastic pressures are individually non-zero at

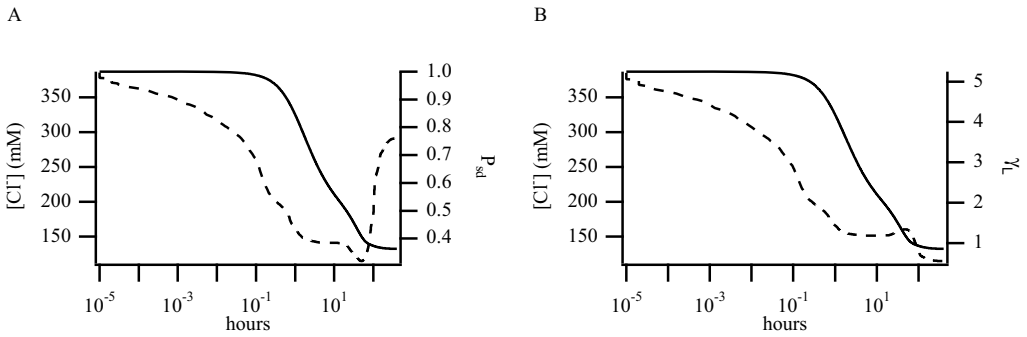

Fig. 5. Effect of lumen volume and stretch-deactivation of the Cl^- channels on $[Cl^-]$. Time is plotted on a logarithmic scale. A: $[Cl^-]$ (solid curve, left axis) and stretch-deactivation of the Cl^- channels (P_{sd}) (dashed curve, right axis). B: $[Cl^-]$ (solid curve, left axis) and γ_L (dashed curve, right axis). The term γ_L is the ratio of the total cell volume to the lumen volume ($w_{cell}c(t)/w_l(t)$).

steady-state. Correspondingly, the lumenal ion concentration is 0.0494 mM higher than the intracellular ion concentration and the difference between the radii, $R_l - R_r$ is 0.568 μm. The individual pressures and ΔP are shown in Fig. 6. The osmotic pressure and elastic pressure are plotted in Panel A. The

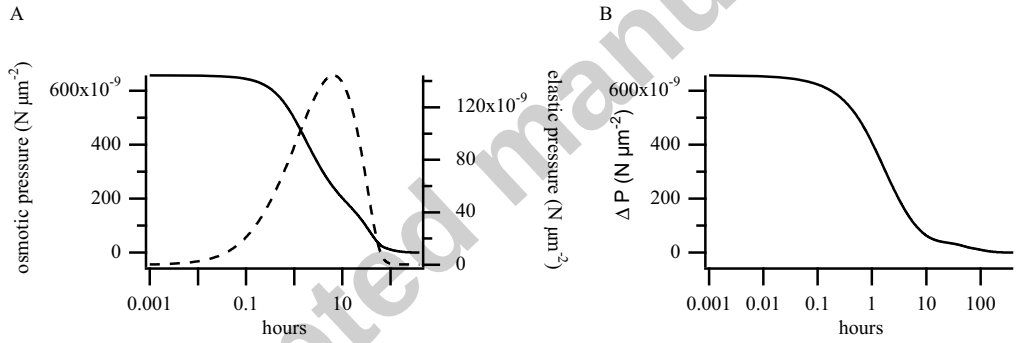

Fig. 6. A: Osmotic pressure (solid curve, left axis) and elastic pressure (dashed curve, right axis). B: ΔP vanishes after approximately 100 hours.

osmotic pressure (solid curve, left axis) increases first, following the increase of Cl^- in the lumen. The osmotic pressure has a dominating effect on the lumen volume on a time scale of minutes after which the elastic pressure increases so that the contributions from both terms become equal.

3.2 Stretch-independent cell proliferation and cell death set equal: $\gamma_d = 0$

Here we consider the case when stretch-independent cell proliferation and cell death are equal, so that the changes in cell number are stretch-induced only. We do this by setting the term $\gamma_d = 0$.

For the same parameter set, we find that the volume again saturates, but at a higher value of 8.24×10^5 μm^3, amounting to a 2.8 fold increase compared to the fitted experimental scenario. The steady-state [Cl^-] saturates at the same value and it is greater cell proliferation which causes a greater lumen increase.

In contrast to the previous case in which γ_d is non-zero, the volume saturates when both the osmotic and elastic pressures are individually zero. This can be seen from the equation for the cell number. In order for steady-state to be achieved, the term ΔA must be zero and this can only be the case when the surface area, $A(t)$, and the surface area covered by the same number of unstretched cells, $c(t)A_{\text{apical}}$, are equal. This implies that the radii $R_l(t)$ and $R_r(t)$ are equal, giving zero elastic pressure. The lumenal [Cl^-] self-adjusts such that the concentration difference between the lumenal compartment and the intracellular space becomes zero, giving zero osmotic pressure.

3.3 Non-saturating lumen volume growth

In this section, we investigate the mechanisms by which the lumen volume increases without bound. We implement two scenarios, first by altering the Cl^- concentration and, second, by considering uncontrolled basal cell proliferation, which is a hallmark of cancerous cells.

First, we assume a fixed [Cl^-] in the lumen and set the chloride equation to zero so that the [Cl^-] remains constant throughout. We simulated the model at two fixed lumenal Cl^- concentrations, 150 mM and 165 mM. Both situations are shown in Fig. 7. For a [Cl^-] of 150 mM the lumen volume first increases, but then decreases to below its initial volume. This is a result of too weak fluid secretion, which is needed to stimulate first volume increase and then cell proliferation, which then drives the second phase of lumen expansion. However, for a [Cl^-] of 165 mM, the lumen volume increases without bound. The osmotic pressure remains high, and there is a constant fluid influx to drive lumen expansion. The two examples are dependent also on the initial cell volume and cell number. For a larger initial lumen volume, a [Cl^-] of 150 mM would result in non-saturation of the lumen volume. In this case, the elastic pressure becomes greater than the osmotic pressure so that the lumen volume decreases.

Alternatively, we can induce non-saturation by modifying cell proliferation. We can mimic this by changing the term $-c(t)\gamma_d$ in the cell proliferation equation to $+c(t)\gamma_d$. This positive contribution implies that cell proliferation outweighs death. The cell number does not saturate and continues to increase so that the lumen volume does not saturate. However, the [Cl^-] does saturate, although at a slightly higher concentration of 136.59 mM. This gives a higher

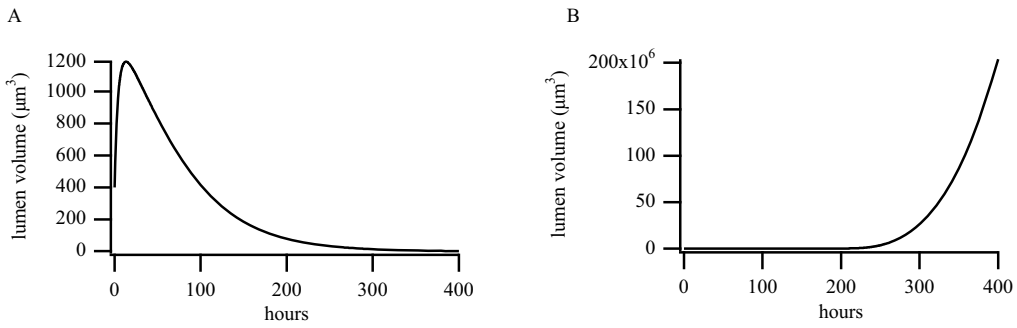

Fig. 7. Lumenal [Cl^-] is fixed throughout the simulation. A: [Cl^-] = 150 mM. The lumen volume first increases, but then decreases below its initial volume. B: [Cl^-] = 165 mM. The lumen volume increases without bound.

concentration difference, $C_{\text{lumen}} - C_{\text{intra}}$ of 4.086 mM, leading to higher osmotic pressure.

3.4 Varying Cl^- influx changes the saturation volume of the lumen

We demonstrate here that the model can be adapted for other systems to include different Cl^- signaling pathways that affect the Cl^- influx into the lumen and thus, the final size of the cyst.

We first show how increasing the Cl^- influx affects the saturation volume of the lumen. Here, we do this by increasing the conductance of the channel, g_{Cl}. The conductance can be voltage dependent or ligand dependent, both of which could change the conductance of the Cl^- channel. Alternatively, as we have not included any specific form for the conductance or the open probability of the channel, P_{Cl}, we could also have increased the open probability. The open probability reflects the gating mechanisms of the channel and thus, could be adapted to include different gating properties for different types of Cl^- channels.

We increased the Cl^- conductance and find that the lumen volume saturates at a higher value with higher Cl^- conductances. Fig. 8 shows the effect of increasing the conductance on the steady state of the lumen volume. Panel A shows the lumen volume increasing linearly with increasing Cl^- conductance. The [Cl^-] settles to the same steady-state concentration, but the steady-state cell number increases with increasing Cl^- conductance. We plot the lumen volume equation for two values of the conductance, $g_{\text{Cl}} = 7.30$ nS (solid curve), and $g_{\text{Cl}} = 73.00$ nS (dashed curve), in Panels B and C. The lumen volume derivative is approximately the same at the initial stage, which is due, as discussed earlier, to the initial [Cl^-]. However, it increases slightly faster for the higher conductance value. The lumen volume derivative then remains higher

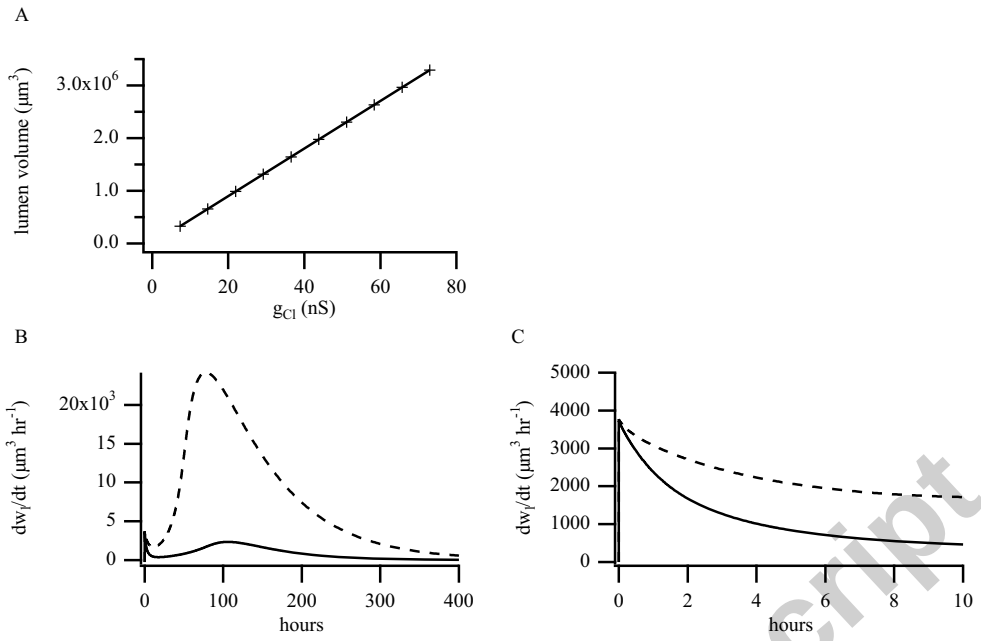

Fig. 8. Effect of increasing the Cl^- conductance, g_{Cl}, on the saturation value of the lumen volume. A: Cl^- conductance is increased up to ten-fold. The saturation volume increases linearly. B: Lumen volume equation as function of time for two different values of g_{Cl}. Solid curve: $g_{Cl} = 7.30$ nS, dashed curve: $g_{Cl} = 73.00$ nS. C: Lumen volume equation for two different values of g_{Cl} shown up to 10 hours.

for longer (Panel C), leading to greater lumen volume growth. This has the effect of increasing cell proliferation, which then feeds back onto the lumen volume growth, as can be seen by the higher second peak of the dashed curve (Panel B). Therefore, by increasing the Cl^- conductance ten-fold, the effect is to increase the saturating lumen volume ten-fold through the interacting volume expansion and increased cell proliferation feedback.

Conversely, by setting the open probability of the channel (P_{Cl}) ten times lower, the lumen volume saturates at 3.17×10^4 μm^3 rather than 3.28×10^7 μm^3. This is in agreement with studies that have shown that when the Cl^- channels are blocked, fluid accumulation within the lumen is inhibited and thus lumen growth is inhibited (Li et al., 2004).

All the above discussed scenarios included the stretch-deactivation mechanism P_{sd} for the Cl^- channel. However, by neglecting this mechanism and setting $P_{sd} = 1$, we find that the lumen volume still saturates, although at a higher value.

4 Discussion

In this study, we investigated the regulatory mechanisms for the control and saturation of cyst lumen growth. To do this, we constructed a model for cell proliferation, ion transport and fluid secretion. We included a stretch-deactivation mechanism of the Cl^- channels and a stretch-induced mechanism for cell proliferation. We chose not to model specific intracellular signaling pathways, intracellular ion exchange processes or cell volume changes and focused instead on the general mechanisms for growth control. The causal chain by which the lumen is increased, as described by our model, can be seen in Fig. 1 and is summarized here:

(1) Build-up of $[Cl^-]$ in the lumen induces an osmotic water flux along its concentration-gradient into the lumen. The lumen volume increases.
(2) An increase in the surface area of the lumen promotes cell proliferation. The Cl^- channels are deactivated in response to the increased stretch.
(3) The $[Cl^-]$ drops as a result of both stretch-deactivation of the Cl^- channels and dilution due to increasing lumen volume. The model predicts that the lumen volume plateaus, but then experiences a second, slower phase of increase due to the increase in cell number.
(4) Saturation of the lumen volume occurs when the combined osmotic and elastic pressure, ΔP is zero.

The increase in lumen volume is initially due to the osmotic pressure, caused by the increased chloride concentration. The increasing volume has the effect to dilute the $[Cl^-]$ so that the influx of the $[Cl^-]$ is balanced by the efflux out of the lumen. The effect of the stretch-deactivation of the Cl^- channels drops, but the $[Cl^-]$ does not increase again, due to the dilution of the concentration. The increasing surface area of the lumen also coincides with a deactivation of the Cl^- channels. When the chloride concentration reaches steady-state, the lumen increase is temporarily arrested. However, an increase in cell proliferation occurs in response to the expanding lumen surface area. The lumen volume begins to increase again, following the cell number increase. Cuppage et al. (1980) and Huseman et al. (1980) found that a balanced state is achieved between proliferation and fluid secretion components of cyst enlargement. This is indicated by the result that hydrostatic pressures within cysts remain close to values observed across the walls of normal renal tubules.

Grantham et al. (2008) developed a mathematical model for renal cyst growth. They chose a simple model where cyst enlargement is determined by the difference between the rate of cell proliferation and apoptosis. They did not include explicit fluid secretion, rather, this was taken to be a by-product of cyst enlargement via cell proliferation. They assumed cell proliferation to be the principal factor of renal cyst enlargement, with fluid secretion only play-

ing a role when the cyst has detached from the parent tubule. In their model cyst volume grows exponentially, growing 10% per year. Their modeling assumption was that the cyst volume was 0.0042 cm^3 at initiation, the cysts remained as spheres and enlarged at a constant rate over the life of the patient. In contrast, our model is capable of emergent growth saturation. The saturation of the lumen volume growth in our model is not linked to any biochemical size regulation pathway. Saturation of the lumen volume occurs when the combined effect of the elastic and osmotic pressure terms is zero.

We are interested in the saturation of lumen growth and this was achieved by our proposed model, but also by the balance of factors such as cell division and cell death. For example, if stretch-independent cell proliferation outweighed cell death (replacing $-\gamma_{\mathrm{d}}c(t)$ by $+\gamma_{\mathrm{d}}c(t)$ in Eq. 6), the lumen volume and cell number do not saturate. However, the $[Cl^-]$ does saturate. In our model, the saturation of the variables emerges from a dynamic balance between different processes. Alternatively, phenomenological approaches model the saturation of tissue growth using a logistic equation to describe the cell number increase as done by Martin et al. (2009) who performed experiments to understand the interactions of cell competition and growth in the *Drosophila* wing disc. Our mechanistic model yields the emergent behavior of saturating cyst growth that could alternatively be obtained by using a logistic equation.

We did not include signaling pathways for cAMP activation as the focus of this study was on the different mechanisms for saturation of lumen volume. It is suggested that cAMP-dependent Cl^- channels may also stimulate cell proliferation via the ERK pathway (Yamaguchi et al., 2003). They found that under the presence of certain inhibitors of ERK activation, cyst growth was greatly reduced. Epithelial cell function can be modulated by the activation, via extracellular ATP, of surface receptors such as the P2Y receptor. They concluded that stimulation of P2Y receptors by extracellular ATP increased the growth of cysts via a cAMP-dependent activation of the ERK pathway. However, Li et al. (2004) found that forskolin, a cAMP agonist, known to stimulate the proliferation of ADPKD epithelial cells, failed to stimulate cell proliferation of MDCK cells. One possible explanation, which they put forward, is that their MDCK cells endogenously produce high levels of intracellular cAMP such that further stimulation by forskolin fails to increase cell proliferation. However, on further observations, they find this not to be the case. Instead, they find their cells to be similar to human kidney cortex epithelial cells where cAMP either has no effect or inhibits cell proliferation. cAMP may stimulate fluid secretion in two ways (Tanner et al., 1992). If it causes a rise in the intracellular pH, the chloride-bicarbonate exchanger may be activated. Secondly, it may increase chloride conductance of the membrane leading to higher fluxes of ions into the lumen. The generality of our model can be adapted to include these cell-specific ion transport mechanisms, which can be used to study the specific causes of ADPKD.

Our present analyses reinforces the importance of ion transport in size regulation. Therefore, attempts to manipulate ion channels in *in vitro* experiments of cyst growth would be instructive. In this present study, we increased the Cl^- conductance, g_{Cl}, and found that this increased the saturation volume of the lumen. We found that the increased saturation volume was due to a higher cell proliferation rate. The effect of increasing the Cl^- conductance was to increase the rate of volume change only slightly. However, this initial slight increase in lumen volume, due to increased Cl^- influx, affected the cell proliferation dramatically. It is this second phase of lumen growth, due to cell proliferation, that causes the lumen volume to saturate at a higher value. We varied the Cl^- conductance, g_{Cl}. Alternatively, we could also have varied the open probability of the channel, which in this model is also constant. Therefore, this model can be modified to include intracellular signaling pathways or voltage dependencies that affect the Cl^- conductance or by including gating mechanisms that control the open probability of the Cl^- channel.

We included stretch-regulation of cell proliferation. This has been studied theoretically by Shraiman (2005) who proposed that the dependence of the rate of cell proliferation could provide a feedback mechanism back to itself, in order to stabilize uniform growth. Hufnagel et al. (2007); Aegerter-Wilmsen et al. (2007) proposed models of *Drosophila* wing imaginal disc growth under the control of mechanical forces. These models account for observations such as uniform growth and both models propose that compression in the center of the disc leads to termination of disc growth. Nienhaus et al. (2009) studied the connections between mechanical stress, growth control and morphogenesis by applying a method of stress-birefringence, which can be considered as maps of mechanical stress, to the wing imaginal disc of *Drosophila*. They found that the stresses are inhomogeneously distributed in the wing disc, with maximum stress in the center of the disc. Their results are in agreement with predictions made by both models of growth under mechanical feedback, (Hufnagel et al., 2007; Aegerter-Wilmsen et al., 2007).

We investigated changes to the cell proliferation rate by modifying the value of γ_d, the net contribution of stretch-independent cell proliferation and cell loss (by death of movement out of the monolayer). In the first case where γ_d was set to zero, the system still saturated, though at higher lumen volume and cell number values. The system is limited by the stretch-dependent cell proliferation rate, which becomes zero when the cell number has increased to cover the increased lumen surface area. In the second case, we took a negative value for γ_d so that cell proliferation outweighed cell loss. Here, the system did not saturate and this can be seen analytically as the cell number equation now only has positive contributions.

89% of the difference in the cyst surface area is due to a higher cell number (Tanner et al., 1995). Because the differences in the surface area mainly reflect

the cell number, the surface area can be used to determine doubling times of cells and Tanner et al. (1995) used this to calculate a doubling time of approximately 50 hours. They calculated this doubling time between day 7 and day 9 after the cyst had been seeded. During this period of 48 hours, the surface area doubled. We calculated our model doubling times and found that the doubling time between 50 and 100 hours is 18.49 hours, between 100 and 150 hours, the doubling time is 61.76 hours and between 150 and 200 hours, the doubling time is 190.77 hours.

We fitted our model to the experimental data of Wang et al. (1990), which were measured at time points of days. Ferrari et al. (2008) also measured cyst lumen volumes, focusing on earlier time points. They investigated the development of single MDCK cells into aggregates and found that initially, the lumen volume increases without changes in the total volume or cell number. From Fig. 6E of their paper, it can be observed, that between 0 and 60 minutes, the lumen volume increased from 60 μm^3 to 150 μm^3, a 2.5 fold increase. From 120 minutes to 240 minutes, the lumen volume increased to 480 μm^3, giving a 3.2 fold increase. From our model simulations, the lumen volume increased from 401 μm^3 to 5370 μm^3 by 120 minutes, a 13 fold increase. From 120 minutes to 240 minutes, the lumen volume increased 1.4 times to 8000 μm^3. In this second phase, our rate of increase is comparable to that seen by Ferrari et al. (2008). Although we did not fit such early data points, our model reproduces results comparable to the measurements of Ferrari et al. (2008). Fitting earlier data measurements would be a logical future step, as the initial lumen expansion is linked to fluid secretion and as can be seen from our simulations, this phase occurs on a very short time scale. This also would benefit from measurements of the lumenal [Cl^-], which is the main driving force for fluid accumulation.

This model is readily applicable to cyst growth in other organs or species. Here we focused on the general mechanisms of fluid secretion and cell proliferation to increase lumen size. Other parameter sets also gave the same two-phase lumen expansion and saturation of the volume. The applicability of the model can contribute to both the understanding and treatment of renal cyst diseases. Even tracheal tubes, which transport oxygen, accumulate fluid in the lumen when the tubes initially form. This fluid is then cleared later (Lubarsky and Krasnow, 2003). Since fluid secretion is also a driving force for tubulogenesis, the model is extendable to tube morphogenesis and development of epithelial organs. Therefore one possible extension is the inclusion of symmetry-breaking mechanisms for tubulogenesis. Altogether, our analysis reinforces the importance of ion regulation for size control.

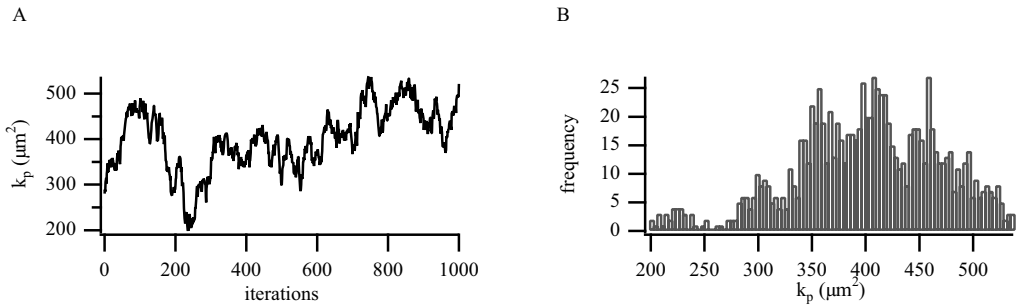

Fig. 9. Example of a parameter convergence, shown for k_p. A: Convergence plot. B: Marginal histogram.

5 Appendix

5.1 Parameter estimation with Bayesian inference and MCMC

We use a Bayesian inference and Markov chain Monte Carlo (MCMC) (Gilks et al., 1996) approach to fit the parameters. In the Bayesian approach, the parameters are assumed to be random variables that follow a particular distribution. Inferences are made based on the posterior distribution of the parameters, given the data and prior information about the parameters. The MCMC method provides a means of generating a sample from the posterior distributions of the parameters given the data. A new realization from the posterior distributions is obtained by sampling a candidate value of the parameter from the proposal distribution. This candidate value is accepted or rejected by comparison of the current parameter value with the candidate value by calculating the ratio of the density at the current and candidate points. Here we use the Metropolis-Hastings algorithm (Metropolis et al., 1953; Hastings, 1970), which generates a Markov chain with equilibrium distribution from the posterior.

We first construct the posterior probability distribution

$$p(q|d) \propto p(q)p(d|q), \tag{20}$$

where $p(\cdot|\cdot)$ denotes a conditional probability, d is the data and q the parameters to be determined. The left hand of Eq. (20) is the quantity in which we are interested. Commonly, in classical statistics, the maximum of $p(q|d)$ would give the set of parameters that maximizes the probability of obtaining the observed data. This likelihood is maximized by methods such as the simplex algorithm or steepest descent to obtain the parameter values that give the maximum probability. The resulting parameters could be interpreted as the "best" choice for those unknowns.

By using Markov chain Monte Carlo (MCMC) techniques, we can construct the entire distribution from which we can extract the maximum, the mean, or any other statistical characterization required. Using these techniques, the distribution of the Markov chain that is generated should converge to the posterior distribution, given by Eq. (20).

The right hand side of Eq. (20) are quantities that we can calculate.

$p(q)$: The prior, $p(q)$ summarizes any prior information we have on the possible values of the parameters. Here we use an uninformative prior for each of the parameters.

$p(d|q)$: We assume that the error at each data point is Gaussian distributed to give

$$p(d|q) \propto \exp\left(\frac{|\tilde{d}_i - d_i|}{2\sigma^2}\right), \tag{21}$$

where the d_i are the experimental values at each ith time and $\tilde{d}_i$ are the estimated values obtained from the set of parameters, q. The variance is given by σ^2 and is estimated from the data. The values for the d_i and σ are given in Table 1 and the i refer to the days on which the measurements were taken. In this case, the $\tilde{d}_i$ are the simulated lumen volumes from the given parameters, q.

A Markov chain with equilibrium distribution $p(q|d)$ is then generated using the Metropolis-Hastings algorithm (Metropolis et al., 1953; Hastings, 1970). New parameter values, q', are randomly drawn from the uniform distribution $U(q-\delta, q+\delta)$, where δ is the size of the random walk. The new candidate parameters are accepted with probability

$$\alpha = \min\{1, \frac{p(d|q')p(q')}{p(d|q)p(q)}\}.$$

If the sampling procedure converges for a particular parameter, then we conclude that the parameter is well-determined by the data. We can calculate the mean and variance of the parameter distribution, giving the mean value of the parameter, and information as to how much it can vary without compromising the fit. An example of a fit for the parameter k_p is given in Fig. 9. Fig. 9A shows the convergence plot for k_p and 9B shows the marginal histogram.

6 Acknowledgments

We are grateful to M. Kücken, A. Meinhardt and A. Deutsch for fruitful discussions and acknowledge support by the German Ministry for Education and Research through grant no. 0315259.

References

Aegerter-Wilmsen, T., Aegerter, C., Hafen, E., Basler., K., 2007. Model for the regulation of size in the wing imaginal disc of drosophila. Mech Dev. 124, 318–326.

Balcarova-Ständer, J., Pfeiffer, S., Fuller, S., Simons, K., 1984. Development of cell surface polarity in the epithelial Madin-Darby canine kidney (MDCK) cell line. EMBO J. 3, 2687–2694.

Belibi, F., Reif, G., Wallace, D., Tamaguchi, T., Olsen, L., Li, H., Jr, G. H., Grantham, J., 2004. Cyclic AMP promotes growth and secretion in human polycystic kidney epithelial cells. Kidney Int. 66, 964–973.

Cuppage, F., Huseman, R., Chapman, A., Grantham, J., 1980. Ultrastucture and function of cysts form from human adult polycystic kidneys. Kidney Int. 17, 372–381.

Eaton, S., Simons, K., 1995. Apical, basal, and lateral cues for epithelial polatization. Cell 82, 5–8.

Elia, N., Lippincott-Schwartz, J., 2009. Culturing MDCD cells in three dimensions for analyzing intracellular dynamics. Curr Protoc Cell Biol. , 4.22.1–4.22.18.

Farinas, J., Verkman, A., 1996. Cell volume and plasma membrane osmotic water permeability in epithelial cell layers measured by interferometry. Biophys. J. 71, 3511–3522.

Ferrari, A., Veligodskiy, A., Berge, U., Lucas, M. S., Kroschewski, R., 2008. ROCK-mediated contractility, tight junctions and channels contribute to the conversion of a preapical patch into apical surface during isochoric lumen initiation. J Cell Sci. 121, 3649–3663.

Fischbarg, J., Li, J., Kuang, K., Echevarria, M., Iserovich, P., 1993. Determination of volume and water permeability of plated cells from measurements of light scattering. Am. J. Physiol. 265, C1412–C1423.

Gilks, W., Richardson, S., Spiegelhalter, D. (Eds.), 1996. Markov chain Monte Carlo in practice. London: Chapman and Hall.

Gin, E., Crampin, E. J., Brown, D. A., Shuttleworth, T. J., Yule, D. I., Sneyd, J., 2007. A mathematical model of fluid secretion from a parotid acinar cell. J. Theor. Biol. 248, 64–80.

Grantham, J., Cook, L., Torres, V., Bost, J., Chapman, A., Harris, P., Guay-Woodford, L., Bae, K., 2008. Determinants of renal volume in autosomal-dominant polycystic kidney disease. Kidney Int. 73, 108–116.

Hanaoka, K., Guggino, W. B., 2000. cAMP regulates cell proliferation and cyst formation in autosomal polycystic kidney disease cells. J. Am. Soc. Nephrol. 11, 1179–1187.

Hastings, W., 1970. Monte Carlo sampling methods using Markov chains and their applications. Biometrika 57, 97–109.

Hufnagel, L., Teleman, A. A., Rouault, H., Cohen, S., Shraiman., B., 2007. On the mechanism of wing size determination in fly development. PNAS 104, 3835–438–0.

Huseman, R., Grady, A., Welling, D., Grantham, J., 1980. Macropuncture study of polycystic disease in adult human kidneys. Kidney Int. 18, 375–385.

Kovbasnjuk, O., Leader, J. P., Weinstein, A. M., Spring, K. R., 1998. Water does not flow across the tight junctions of MDCK cell epithelium. PNAS 95, 6526–6530.

Kücken, M., Soriano, J., Pullarkat, P. A., Ott, A., Nicola, E. M., 2008. An osmoregulatory basis for shape oscillations in regenerating *Hydra*. Biophys. J. 95, 978–985.

Li, H., Findlay, I. A., Sheppard, D. N., 2004. The relationship between cell proliferation, Cl^- secretion and renal cyst growth: a study using CFTR inhibitors. Kidney Int. 66, 1926–1938.

Liu, M., Xu, J., Tanswell, A., Post, M., 1993. Stretch-induced growth-promotin activites stimulate fetal rate lung epithelial cell proliferation. Exp. Lung. Res. 19, 505–517.

Lubarsky, B., Krasnow, M. A., 2003. Tube morphogenesis: making and shaping biological tubes. Cell 112, 19–28.

Mangoo-Karim, R., Uchic, M., Lechene, C., Grantham, J. J., 1989. Renal epithelial cyst formation and enlargement *in vitro*: dependence on cAMP. PNAS 86, 6007–6011.

Martin, F. A., Herrera, S. C., Morata, G., 2009. Cell competition, growth and size control in the *Drosophila* wing imaginal disc. Development 136, 3747–3756.

McAteer, J., Evan, A., Gardner, E., 1987. Morphogenetic clonal growth of kidney epithelial cell line MDCK. Anat. Rec. 217, 229–239.

Metropolis, N., Rosenbluth, A., Rosenbluth, M., Teller, A., Teller, E., 1953. Equations of state calculations by fast computing machines. J. Chem. Phys. 21, 1087–1092.

Nienhaus, U., Aegerter-Wilmsen, T., Aegerter., C. M., 2009. Determination of mechanical stress distribution in drosophila wing discs using photoelasticity. Mech Dev. 126, 942–949.

O'Brien, L. E., Zegers, M., Mostov, K., 2002. Building epithelial architecture: insights from three-dimensional culture models. Nat Rev Mol Cell Biol. 3, 531–537.

Rivers, R. L., McAteer, J. A., Clendenon, J. L., Connors, B. A., Evan, A. P., James C. Williams, J., 1996. Apical membrane permeability of MDCK cells. Am. J. Physiol. 271, C226–C34.

Sardini, A., JS, J. A., Weylandt, K., Nobles, M., MA, M. V., Higgins, C., 2003. Cell volume regulation and welling-activated chloride channels. Biochim Biophys Acta. Dec 30;1618(2): 1618, 153–162.

Shraiman, B. I., 2005. Mechanical feedback as a possible regulator of tissue growth. PNAS 102, 3318–3323.

Stefani, E., Cereijido, M., 1983. Electrical properties of cultured epithelial cells (MDCK). J Membrane Biol. 73, 177–184.

Sullivan, L. P., Wallace, D. P., Grantham, J. J., 1998a. Chloride and fluid

secretion in polycystic kidney disease. J. Am. Soc. Nephrol. 9 903-16, 903–916.

Sullivan, L. P., Wallace, D. P., Grantham, J. J., 1998b. Epithelial transport in polycystic kidney disease. Physiol. Rev. 78, 1165–1191.

Tan, J., Tien, J., Pirone, D., Gray, D., Bhadriraju, K., Chen, C., 2003. Cells lying on a bed of microneedles: an approach to isolate mechanical force. Proc Natl Acad Sci U S A. 100, 1484–1489.

Tanner, G. A., Maxwell, M. R., McAteer, J. A., 1992. Fluid transport in a cultured cell model of kidney epithelial cyst enlargement. J. Am. Soc. Nephrol. 2, 1208–1218.

Tanner, G. A., McQuillan, P. F., Maxwell, M. R., Keck, J. K., McAteer, J. A., 1995. An *in vitro* test of the cell stretch-proliferation hypothesis of renal cyst enlargement. J. Am. Soc. Nephrol. 6, 1230–1241.

Timbs, M., Spring, K., 1996. Hydraulic properties of MDCK cell epithelium. J. Membrane. Biol. 153, 1–11.

Wang, A. Z., Ojakian, G. K., Nelson, W. J., 1990. Steps in the morphogenesis of a polarized epithelium. I. Uncoupling the roles of cell-cell and cell-substratum contact in establishing plasma membrane polarity in multicellular epithelial (MDCK) cysts. J. Cell. Sci. 95, 137–151.

Yamaguchi, T., Nagao, S., Wallace, D., Belibi, F., Cowley, B., Pelling, J., Grantham, J., 2003. Cyclic AMP activates B-Raf and ERK in cyst epithelial cells from autosomal-dominant polycystic kidneys. Kidney Int. 63, 1983–1994.

Yamaguchi, T., Pelling, J., Ramaswamy, N., Eppler, J., Wallace, D., Nagao, S., Rome, L., Sullivan, L., Grantham, J., 2000. cAMP stimulates the in vitro proliferation of renal cyst epithelial cells by activating the extracellular signal-regulated kinase pathway. Kidney Int. 57, 1460–1471.

Zeng, D., Ferrari, A., Ulmer, J., Veligodskiy, A., Fischer, P., Spatz, J., Ventikos, Y., Poulikakos, D., Kroschewski., R., 2008. Three-dimensional modeling of mechanical forces in the extracellular matrix during epithelial lumen formation. Biophys. J. 90, 4380–4391.